Genetic analysis suggests a surface of PAT-4 (ILK) that interacts with UNC-112 (kindlin)

Hiroshi Qadota (ID) ,[1] Annie McPherson,[1] Rachel Corbitt,[1] Evan Kelton Dackowski,[1] Yohei Matsunaga,[1] Andres F. Oberhauser (ID) ,[2] and Guy M. Benian (ID) [1,*]

[1]Department of Pathology, Emory University, Atlanta, GA 30322, USA,
[2]Department of Neuroscience, Cell Biology and Anatomy, University of Texas Medical Branch, Galveston, TX 77555, USA

*Corresponding author: Department of Pathology, Emory University, Atlanta, GA 30322, USA. Email: pathgb@emory.edu

Abstract

Integrin plays a crucial role in the attachment of cells to the extracellular matrix. Integrin recruits many proteins intracellularly, including a 4-protein complex (kindlin, ILK, PINCH, and parvin). *Caenorhabditis elegans* muscle provides an excellent model to study integrin adhesion complexes. In *Caenorhabditis elegans*, UNC-112 (kindlin) binds to the cytoplasmic tail of PAT-3 (β-integrin) and to PAT-4 (ILK). We previously reported that PAT-4 binding to UNC-112 is essential for the binding of UNC-112 to PAT-3. Although there are crystal structures for ILK and a kindlin, there is no co-crystal structure available. To understand the molecular interaction between PAT-4 and UNC-112, we took a genetic approach. First, using a yeast 2-hybrid method, we isolated mutant PAT-4 proteins that cannot bind to UNC-112 and then isolated suppressor mutant UNC-112 proteins that restore interaction with mutant PAT-4 proteins. Second, we demonstrated that these mutant PAT-4 proteins cannot localize to attachment structures in nematode muscle, but upon co-expression of an UNC-112 suppressor mutant protein, mutant PAT-4 proteins could localize to attachment structures. Third, overexpression of a PAT-4 mutant results in the disorganization of adhesion plaques at muscle cell boundaries and co-expression of the UNC-112 suppressor mutant protein alleviates this defect. Thus, we demonstrate that UNC-112 binding to PAT-4 is required for the localization and function of PAT-4 in integrin adhesion complexes in vivo. The missense mutations were mapped onto homology models of PAT-4 and UNC-112, and taking into account previously isolated mutations, we suggest a surface of PAT-4 that binds to UNC-112.

Keywords: integrin; integrin adhesion complex; mutant screening; suppressor; KIPP complex

Introduction

Caenorhabditis elegans muscle used for locomotion is located in the body wall and consists of 95 spindle-shaped mononuclear cells arranged in interlocking pairs that run the length of the animal in 4 quadrants. The myofibrils are restricted to a narrow ~1.5-μm zone adjacent to the cell membrane along the outer side of the muscle cell. The thin filaments are attached to dense bodies (Z-disk analogs), and the center of the bundle of thick filaments (A-bands) are attached to M-lines. Moreover, all of the dense bodies and M-lines are anchored to the muscle cell membrane and extracellular matrix, which is attached to the hypodermis and cuticle. This allows the force of muscle contraction to be transmitted directly to the cuticle and allows movement of the whole animal (Waterston 1988; Moerman and Fire 1997; Moerman and Williams 2006; Gieseler *et al.* 2017). Thus, nematode muscle M-lines and dense bodies serve the function of analogous sarcomeric structures in vertebrate muscle. However, because these structures are attached to the cell membrane and contain integrin and integrin-associated proteins (see below), they also act as costameres of vertebrate muscle and focal adhesions of nonmuscle cells.

The membrane-proximal regions of the dense bodies and M-lines consist of integrin and associated proteins (Moerman and Williams 2006; Gieseler *et al.* 2017). Integrin-associated proteins are also used at the adhesion plaques that lie between adjacent muscle cells and are likely involved in transmitting forces laterally (Moody *et al.* 2020). The cytoplasmic tail of β-integrin (PAT-3) is associated with 4 conserved proteins: UNC-112 (kindlin), PAT-4 [integrin-linked kinase (ILK)], PAT-6 (α-parvin), and UNC-97 (PINCH). The cytoplasmic tail of PAT-3 (β-integrin) binds to UNC-112, and UNC-112 binds to PAT-4 (Mackinnon *et al.* 2002; Qadota *et al.* 2012). PAT-4 also has been shown to interact with PAT-6 and UNC-97 (Mackinnon *et al.* 2002; Lin *et al.* 2003; Norman *et al.* 2007). Each of these proteins is required for myofibril assembly in embryonic and adult muscle (Williams and Waterston 1994; Hobert *et al.* 1999). All 5 proteins are localized to integrin adhesion sites (M-lines, dense bodies, and muscle cell boundaries) in muscle cells (Hobert *et al.* 1999; Rogalski *et al.* 2000; Mackinnon *et al.* 2002; Lin *et al.* 2003; Norman *et al.* 2007; Qadota *et al.* 2017). UNC-112 co-precipitates with PAT-4, PAT-6, and UNC-97, consistent with a 4-protein complex in vivo (Qadota *et al.* 2014).

We have suggested a model for the assembly of integrin-associated proteins previously (Qadota *et al.* 2012): (i) PAT-4 binding to UNC-112 changes the conformation of UNC-112 from closed (inactive) to open (active), (ii) the UNC-112-PAT-4 complex binds to the cytoplasmic tail of PAT-3 (β-integrin), and (iii) PAT-4

recruits PAT-6 and UNC-97. Within this integrin–integrin-associated protein complex, the UNC-112/PAT-4 complex functions as a core. Previously, we reported mutations in UNC-112 that cannot bind to PAT-4 (Qadota et al. 2012), and its extragenic suppressor mutations in PAT-4 (Qadota et al. 2014). These mutations are useful for understanding the interaction surface between UNC-112 and PAT-4 (Qadota and Benian 2014), especially because, although crystal structures for an ILK and a kindlin have been reported, to date, there is no kindlin/ILK (or UNC-112/PAT-4) co-crystal structure. To obtain more molecular information about the UNC-112/PAT-4 interaction, in this study, using a yeast 2-hybrid method, we obtained mutant PAT-4 proteins that cannot bind to UNC-112 and then isolated mutant UNC-112 proteins that can restore the interaction. We then expressed in C. elegans, these mutant PAT-4 and suppressor mutant UNC-112 proteins using a heat shock promoter. After transient expression (2 h of heat shock), we examined muscle localization of mutant PAT-4 with and without suppressor UNC-112. After sustained expression (24 h of heat shock) of these mutant proteins, we examined the organization of muscle adhesion complexes. We found that mutant PAT-4 proteins that cannot bind to UNC-112 fail to localize to muscle attachment structures. However, upon co-expression of suppressor mutant UNC-112 proteins that restore the binding, localization of mutant PAT-4 proteins to attachment structures is restored. We also found that overexpression of a mutant PAT-4 protein results in the disorganization of adhesion plaques at the muscle cell boundary, and co-expression of a suppressor mutant UNC-112 alleviates this defect. The missense mutations were mapped onto homology models of PAT-4 and UNC-112, and taking into account previously isolated mutations, we suggest a surface of PAT-4 that binds to UNC-112.

Materials and methods
Screening for PAT-4 mutants that cannot bind to UNC-112

Mutations in PAT-4 were introduced randomly by error-prone PCR. We PCR-amplified full-length PAT-4 cDNA by an error-prone method (Qadota et al. 2012) using the following primers: 5′ (GAA GAT ACC CCA CCA AAC) and 3′ (AAA GAA GGC AAA ACG ATG) and a PAT-4 cDNA plasmid (pDM#280) (Qadota et al. 2012) as a template. These primers contain 30 base pairs of sequence that overlap regions in the acceptor plasmid. Cloning of error-prone PCR-amplified fragments into the acceptor plasmid was performed by exploiting yeast recombination in vivo (Takita et al. 1997). The mixture of the amplified PCR fragments (1 μg) and the acceptor plasmid (pACT; 1 μg) digested with XhoI was transformed into PJ69-4A harboring pGBDU-PAT-6. Transformed yeast cells were spread onto −Leu −Ura −His plates containing 2 mM 3-amino-1,2,4-triazole for identifying His$^+$ colonies. LEU2 was the marker for the prey plasmid pACT-PAT-4; URA3 was the marker for the bait plasmid pGBDU-PAT-6; and HIS3 was the first marker for the detection of the yeast 2-hybrid interaction. His$^+$ selection ensured that the mutagenized PAT-4 could still interact with PAT-6. This step was essential for eliminating clones with premature stop mutations or with many other mutations. Because His$^+$ selection yields a high level of false positives, ADE2 was used as a second marker for the detection of the yeast 2-hybrid interaction. Thus, His$^+$ colonies were streaked onto an −Ade plate and screened for His$^+$Ade$^+$ colonies. After streaking on a 5-fluoroorotic acid plate to eliminate the URA3 marker bait plasmid (pGBDU-PAT-6), prey clones were isolated from yeast and amplified in Escherichia coli. From a total of 48 His$^+$Ade$^+$ yeast colonies,

47 mutagenized clones were isolated. These prey clones were transformed separately into PJ69-4A carrying either pGBDU-PAT-6 or pGBDU-UNC-112 (full-length) to confirm interaction with PAT-6 and screen for the lack of interaction with UNC-112. Among 47 mutagenized PAT-4 clones, all 47 showed binding to PAT-6, but 16 of these clones could not bind to full-length UNC-112. DNA sequencing of these clones revealed the mutations (Table 1).

Expression of HA-tagged PAT-4 wild type and mutants in C. elegans using heat shock promoters

Full-length PAT-4 cDNA without mutations, or with mutations Q308H, and I432F were amplified by PCR using primers: EcoRV-PAT-4 (GCG GAT ATC ATG TCT TTG TCG ACT CAT TAC) and PAT-4-XhoI (CGC CTC GAG TCA TAA TAT CAT TCT CTC TAA) and cloned into the HA-tag vector, pKS-HA(Nhex2). From these pKS-HA (Nhex2) clones, NheI fragments (containing HA-tagged PAT-4 cDNAs) were cloned into the NheI site of C. elegans expression vectors, pPD49.78 and pPD49.83 (gifts from Dr. Andrew Fire, Stanford University). These vectors contain 2 different heat shock promoters. pPD49.78/83-HA-PAT-4 (wild type, Q308H, and I432F) were mixed with pTG96 (SUR-5::NLS::GFP) as a transformation marker (Yochem et al. 1998) and injected into wild-type N2 worms. Transgenic lines with extrachromosomal arrays containing pPD49.78/83-HA-PAT-4 [wild type (called sfEx56), Q308H (called sfEx54), and I432F (called sfEx55)] and pTG96 were established by picking GFP-positive worms using a GFP dissection microscope. Expression of the HA-tagged PAT-4 proteins (wild type, Q308H, and I432F) was induced by incubation of the transgenic worms at 30°C for 2 h (heat shock). We prepared worm lysates (Hannak et al. 2002) from transgenic worms with or without heat shock and examined the expression of HA-tagged PAT-4 proteins by Western blot, reacting with anti-HA (Sigma-Aldrich H3663; 1:200 dilution).

Screening for UNC-112 mutants that restore binding to PAT-4 Q308H or PAT-4 I432F

We utilized random mutagenesis by PCR, as described previously (Qadota et al. 2014). UNC-112 cDNAs with mutations were amplified with 2 primers [U112-P1 (GCG GGA TCC TCG AGA GTT CAC TCT TGT TGA AG) and U112-2 (CGC CTC GAG AGA TCT GAT CGT CTG TTA AGA)] and a UNC-112 cDNA plasmid (P13-5) (Qadota

Table 1. PAT-4 mutants that cannot bind to UNC-112.

Name	Amino acid changes in PAT-4					
m8	N29S					
m22	Q308H					
m38	M464V					
m43	I432F					
m46	G227V	A388T				
m40	F262Y	M444V				
m17	S300G	A379V	E422G			
m35	L210P	G307R	P448T			
m36	V21E	V35D	H42L	L439F		
m24	K107R	T214S	D251G	G423S		
m32	P15L	C146R	L165S	G231A		
m30	M151K	T203P	N232S	D389N	P459S	
m39	L44P	T86S	G227V	V303A	R318S	D409Y
m33	M18K	H63Y	I213T	V235E	Q242H	P277L	Q299L
m44	E41G	K102E	K191N	T214S	Y293F	Q308H	S325C	E345V	A365V
m48	A67V	F126L	I248V	H306Q	L326M	K356I	I385N	E422V	H427R

Yellow represents single mutations. Blue represents amino acid changes found in 2 independent clones. Pink represents residues mutated in 2 independent clones, but those changes result in different amino acid substitutions.

et al. 2012) as a template. An amplified cDNA and digested vector (pGAD-C3 with BamHI and BglII) were co-transformed into PJ69-4A yeast strain with pGBDU-PAT-4 with Q308H or I432F (UNC-112 nonbinding mutations) and then transformants were spread onto −His plates. To construct pGBDU-PAT-4 with Q308H or I432F, XhoI fragments of mutant m22 (for Q308H) and m43 (for I432F) were cloned into the pGBDU-C2 XhoI site. A total of 30,000 colonies were screened for suppressors of PAT-4 Q308H. After 3 days of incubation at 30°C, His⁺ colonies were 151. Among these 151, 54 clones were isolated and tested for binding to PAT-4 (Q308H). Among 54 isolated clones, 8 clones retained their ability to bind to PAT-4 (Q308H), and the DNA sequences of these clones were determined (Table 2). A total of 846,000 colonies were screened for suppressors of PAT-4 I432F. After 3 days of incubation at 30°C, His⁺ colonies were 107. Among 107, 54 clones were isolated and tested for binding to PAT-4 (I432F). Among 54 isolated clones, 14 clones retained their ability to bind to PAT-4 (I432F), and the DNA sequences of these clones were determined (Table 2). As shown in Table 2, several suppressor mutant UNC-112 clones contained multiple mutations. Among them, 2 clones had 2 mutations each, namely m22-4-9 (Q27R and F117S) and m43-5-33 (N37S and S185T). From this set of 4 mutations, to create clones with single amino acid changes, the following primers were used: for UNC-112 (N37S), TGT CCT TGG AAA TCT TAG TGT GGG AGG ACT CAT GC and GCA TGA GTC CTC CCA CAC TAA GAT TTC CAA GGA CA; for UNC-112 (S185T), CAA TCT TTG CTT CTC AAA CGA ATC TTG ATA TGC GC and GCG CAT ATC AAG ATT CGT TTG AGA AGC AAA GAT TG; for UNC-112 (Q27R), CAC CGA TTT GAA TAT TCG AAG AAG CAT CTC TGT CC and GGA CAG AGA TGC TTC TTC GAA TAT TCA AAT CGG TG; and for UNC-112 (F117S), TTT CTC GGT AAA TTC ATC CAA AGC AAC AAA GAA AT and ATT TCT TTG TTG CTT TGG ATG AAT TTA CCG AGA AA. UNC-112 N-

terminal fragments with site-directed mutations were confirmed by DNA sequencing, then cloned into pGAD-C3 and tested for binding to PAT-4 (Q308H) and PAT-4 (I432F) by the yeast 2-hybrid system.

Co-expression of HA-tagged PAT-4 and myc-tagged UNC-112 in *C. elegans* using heat shock promoters

To create the full-length UNC-112 with the F301S mutation, a BamHI-BglII fragment of the m43-4-4 clone was inserted into pACT-Q-UNC-112-34 (acceptor plasmid for UNC-112 mutagenesis) (Qadota *et al.* 2012), resulting in pACT-UNC-112 (F301S). XhoI fragments of UNC-112 cDNA of either wild type (P13-5) or from pACT-UNC-112 (F301S) were cloned into the SalI site of pGBDU-C2, resulting in pGBDU-UNC-112 (wild type or F301S). The SmaI-BglII fragment of pGBDU-UNC-112 (wild type or F301S) was ligated into pBS-myc (kindly provided from Dr. Kozo Kaibuchi, Nagoya University) via the SmaI and BamHI sites, resulting in pBS-myc-UNC-112 (wild type or F301S). To construct pPD49.78- or pPD49.83-myc-UNC-112 plasmids, the SpeI fragment of pBS-myc-UNC-112 (wild type or F301S) was cloned into pPD49.78 or pPD49.83 (gifts from Dr. Andrew Fire, Stanford University) via a NheI site. These vectors contain 2 different heat shock promoters. pPD49.78/83-HA-PAT-4 (I432F) and pPD49.78/83-myc-UNC-112 (wild type or F301S) were mixed with pTG96 (SUR-5::NLS::GFP) as a transformation marker and injected into wild-type N2 worms. Transgenic lines with extrachromosomal arrays containing pPD49.78/83-HA-PAT-4 (I432F)/pPD49.78/83-myc-UNC-112 (wild type) (called *sfEx60*) or pPD49.78/83-HA-UNC-PAT-4 (I432F)/pPD49.78/83-myc-UNC-112 (F301S) (called *sfEx61*) and pTG96 were established by picking up GFP-positive worms using a GFP dissection microscope. Expression of HA-tagged PAT-4 (I432F) and myc-tagged UNC-112 (wild type or F301S) proteins was induced by incubation of the transgenic worms at 30°C for 2 h (heat shock). We prepared Laemmli-soluble protein extracts (Hannak *et al.* 2002) from these transgenic nematodes with or without heat shock and verified the expression of HA-tagged PAT-4 and myc-tagged UNC-112 proteins by Western blotting, reacting with anti-HA (Sigma-Aldrich H3663, 1/200 dilution) and anti-myc (Sigma-Aldrich H5546, 1/200 dilution).

Integration of transgenic arrays

The extrachromosomal arrays containing pPD49.78/83-HA-PAT-4 (wild type) with pTG96, pPD49.78/83-HA-PAT-4 (I432F) with pTG96, pPD49.78/83-HA-UNC-PAT-4 (I432F)/pPD49.78/83-myc-UNC-112 wild type with pTG96, and pPD49.78/83-HA-UNC-PAT-4 (I432F)/pPD49.78/83-myc-UNC-112 (F301S) with pTG96 were integrated into the genome by ultraviolet irradiation (Mitani 1995) with some modifications (P. Barrett, personal communication). The resulting integrated nematode lines are called *sfIs14*, for pPD49.78/83-HA-PAT-4 (wild type); *sfIs15*, for pPD49.78/83-HA-PAT-4 (I432F); *sfIs16*, for pPD49.78/83-HA-UNC-PAT-4 (I432F)/pPD49.78/83-myc-UNC-112 wild type; and *sfIs17*, for pPD49.78/83-HA-UNC-PAT-4 (I432F)/pPD49.78/83-myc-UNC-112 (F301S). For Supplementary Fig. 2, worm lysates from these integrated lines were examined for the expression of both endogenous PAT-4 and heat shock induced HA-PAT-4 by western blot using antibodies to PAT-4 (Qadota *et al.* 2012) at 1:200 dilution.

Sustained heat shock overexpression

To investigate the effect of expression of PAT-4 wild type, PAT-4 I432F, and PAT-4 I432F/UNC-112 F301S on muscle organization, wild-type worms and worms containing integrated arrays (*sfIs14*,

Table 2. UNC-112N mutants that restore binding to PAT-4 mutants.

Suppressors of PAT-4 Q308H

Mutant	Amino acid changes in UNC-112						
m22-1-1	A96V						
m22-4-9	Q27R	F117S					
m22-2-33	V21I	E134D	L362P				
m22-4-10	P214A	Q333E	I338T				
m22-3-18	K118E	S261T	V279E	V325A			
m22-4-17	K118E	L219S	T233R	V272A			
m22-4-18	R73Q	N115T	A178T	L330P			
m22-4-4	S9P	L33F	E44Q	E84D			
m22-1-13	F117L	E250V	F301L	F315I	Q357H		
m22-2-34	L33F	E44Q	G165R	F310S	Y331H		
m22-6-5	L33S	V51D	E52D	Q86R	S291P	E371G	
m22-4-11	S29C	Q78E	A96V	S267R	N319S	L393H	
m22-3-21	Q104R	M156L	D232G	H216N	S291P	L330P	L340P	E370D
m22-5-34	Contains 1,029–1,196 only						

Suppressors of PAT-4 I432F

Mutant	Amino acid changes in UNC-112						
m43-4-4	F301S						
m43-5-33	N37S	S185T					
m43-6-4	S116L	Y131C	R293K				
m43-5-19	V38I	M42L	I284V	F316L			
m43-3-40	K118E	S136A	T351P	R395S	S397L		
m43-5-35	S56T	R73Q	Q86L	L187F	S291P	N314D	R395G

Yellow represents single mutations. Blue represents amino acid changes found in 2 independent clones. Pink represents residues mutated in 2 independent clones, but those changes result in different amino acid substitutions.

sfIs15, and *sfIs17)* were exposed to 30°C for 24 h. Worms were fixed using the method described below and immunostained with anti-PAT-6 (to examine M-lines, dense bodies, and cell boundaries).

Immunostaining

Worms were fixed using the method described previously (Nonet *et al.* 1993; Wilson *et al.* 2012). Antibody staining with anti-HA (Sigma Aldrich H3663; 1:200 dilution), anti-GFP (Invitrogen A11122, 1:200 dilution), anti-UNC-95 (1:100 dilution; Qadota *et al.* 2007), and anti-PAT-6 (1:100 dilution; Warner *et al.* 2013) was performed as described previously (Qadota *et al.* 2007). Secondary antibodies were anti-rabbit Alexa 488 (Invitrogen) for anti-UNC-95 and anti-GFP, anti-mouse Alexa 594 (Invitrogen) for anti-HA, and anti-rat Alexa 594 (Invitrogen) for anti-PAT-6, each used at 1:200 dilution. Samples were placed on a glass slide with a coverslip containing mounting solution (20 mM Tris (pH 8.0), 0.2 mM DABCO, and 90% glycerol). Images were captured at room temperature with a Zeiss confocal system (LSM510) equipped with an Axiovert 100M microscope and an Apochromat ×63/1.4 numerical aperture oil objective, in ×2.5 zoom mode for Figs. 2 and 4, and no zoom mode for Fig. 5. Super-resolution microscopy (SIM) was performed with a Nikon N-SIM system in 3D-structured illumination mode on an Eclipse Ti-E microscope equipped with a 100×/1.49 NA oil immersion objective, a 561-nm solid-state laser and an EM-CCD camera (DU-897, Andor Technology). Super-resolution images were reconstructed using the N-SIM module in NIS-Elements software. For all the images, confocal and SIM, the color balances were adjusted by using Adobe Photoshop (Adobe, San Jose, CA, USA).

3D modeling

For UNC-112 and PAT-4 structure modeling, SWISS-MODEL (Waterhouse *et al.* 2018) and Phyre2 (Kelley *et al.* 2015) online tools were used. Human kindlin-3 (7C3M.pdb; Bu *et al.* 2020), human ILK (3KMW.pdb; Fukuda *et al.* 2009), and human alpha-parvin (3KMW.pdb; Fukuda *et al.* 2009) were used as reference crystal structures. The homology model of PAT-4 bound to the CH domain of PAT-6 was based on the human ILK/alpha-parvin complex structure (3KMW.pdb; Fukuda *et al.* 2009). The Molecular graphics were generated by using Chimera (Pettersen *et al.* 2004). Single amino acid mutations were inserted using the rotamer tool and then energy minimized in Chimera to minimize interatomic clashes and contacts based on van der Waals radii.

Results

Identification of PAT-4 mutants that cannot bind to UNC-112

To gain further insight into the in vivo significance of interaction between PAT-4 (ILK) and UNC-112 (kindlin), we isolated missense mutations in PAT-4 that result in lack of binding to UNC-112 using the yeast 2 hybrid system. Using an error-prone PCR approach for generating random mutations, we isolated 16 mutant clones (Table 1). We found that among the 16 clones, 4 clones contain single amino acid changes (N29S, Q308H, I432F, and M464V) (Table 1 and Fig. 1a). Each mutant PAT-4 protein fails to bind to UNC-112, but can still bind to PAT-6 (α-parvin). Three of these 4 mutations reside in residues located in the "pseudo kinase" domain, as shown (Q308H, I432F, and M464V) (Fig. 1, a and b). As reported previously, the PAT-4 pseudo kinase domain is essential for binding to UNC-112 (Mackinnon *et al.* 2002). Since N29S is located outside of the pseudo kinase domain, and there is no

crystal structure of ILK or PAT-4 that includes this region, we did not characterize this mutant further. Q308, I432, and M464 are conserved in the human ILK sequence (Supplemental Fig. 1). We generated a homology model of the PAT-4 pseudo kinase domain structure based on the crystal structure of the ILK/parvin complex (Fukuda *et al.* 2009). According to this homology model, Q308, I432, and M464 are located along the same protein surface (Fig. 1c; shown in green). In fact, this surface also contains several residues (I261, F262 and A433) that when mutated permit binding of PAT-4 to UNC-112 D382V (Qadota *et al.* 2014; shown in red in Fig. 1c), and do not overlap with the binding surface of ILK for parvin (Fukuda *et al.* 2009). Q308 is located on an α helix (Fig. 1b), and using the program Chimera, upon mutation to histidine, we found no clashes with neighboring side chains, and this change from polar to a larger polar side chain is predicted to change the local but not the global structure of PAT-4. I432 is located on a loop, and the conservative substitution I432F is predicted to have a minimal effect on either local or global structure using Chimera. M464 is located on the terminal loop, and replacement with valine is also predicted not to affect structure. Since M464 is located C-terminal of the pseudokinase domain (ending with residue 461 as predicted by PFAM), we decided not to characterize it further. Note that position of 1 nonbinding mutation, I432 (green in Fig. 1c), is next to the amino acid residue A433 (red in Fig. 1c) that when mutated to serine can restore the binding of PAT-4 to UNC-112 D382V [Qadota *et al.* 2014; Figs. 1c and 6 (with circle)].

PAT-4 mutant proteins that cannot bind to UNC-112 do not localize to muscle integrin adhesion complexes

To examine whether the Q308H or I432F mutations affect the localization of PAT-4 in *C. elegans* muscle, we created transgenic animals expressing HA tagged wild type or mutant PAT-4 proteins. Expression of HA tagged PAT-4 (wild type, Q308H, and I432F) was confirmed by western blot, and was strictly controlled by the heat shock promoters of our constructs (Fig. 2a). The level of heat-shock induced expression of HA-PAT-4 was found to be equivalent to the level of endogenous PAT-4 (Supplementary Fig. 2). After heat shock, transgenic animals were immunostained with anti-HA (to localize HA tagged PAT-4) and anti-UNC-95 [to identify muscle integrin adhesion complex (IAC) structures]. HA-PAT-4 wild type localized to dense bodies and M-lines, similar to the localization of endogenous PAT-4 determined by use of anti-PAT-4 antibodies (Qadota *et al.* 2017). HA-PAT-4 wild type localized to dense bodies and M-lines similar to UNC-95, but HA-PAT-4 Q308H and HA-PAT-4 I432F did not localize to dense bodies and M-lines (Fig. 2b). These results suggest that PAT-4 localization at muscle attachment structures requires binding to UNC-112 and since these animals express endogenous levels of PAT-6 (α-parvin), the interaction of PAT-4 (ILK) to PAT-6 (α-parvin) is not sufficient for proper localization of PAT-4 (ILK).

Identification of UNC-112 mutants that can restore binding to PAT-4 (Q308H) or PAT-4 (I432F)

To confirm the possibility that UNC-112 binding is sufficient for the proper localization of PAT-4 to muscle IACs, using yeast 2-hybrid screening, we isolated UNC-112 suppressor mutations that restore the ability of PAT-4 Q308H or I432F mutant proteins to interact with UNC-112. It has been reported that only the N-terminal half of UNC-112 is required for the ability of UNC-112 to bind to PAT-4 (Mackinnon *et al.* 2002). Therefore, we mutagenized only the N-terminal half of UNC-112 to screen for suppressor mutations. From suppressor screening of PAT-4 Q308H, we isolated 6
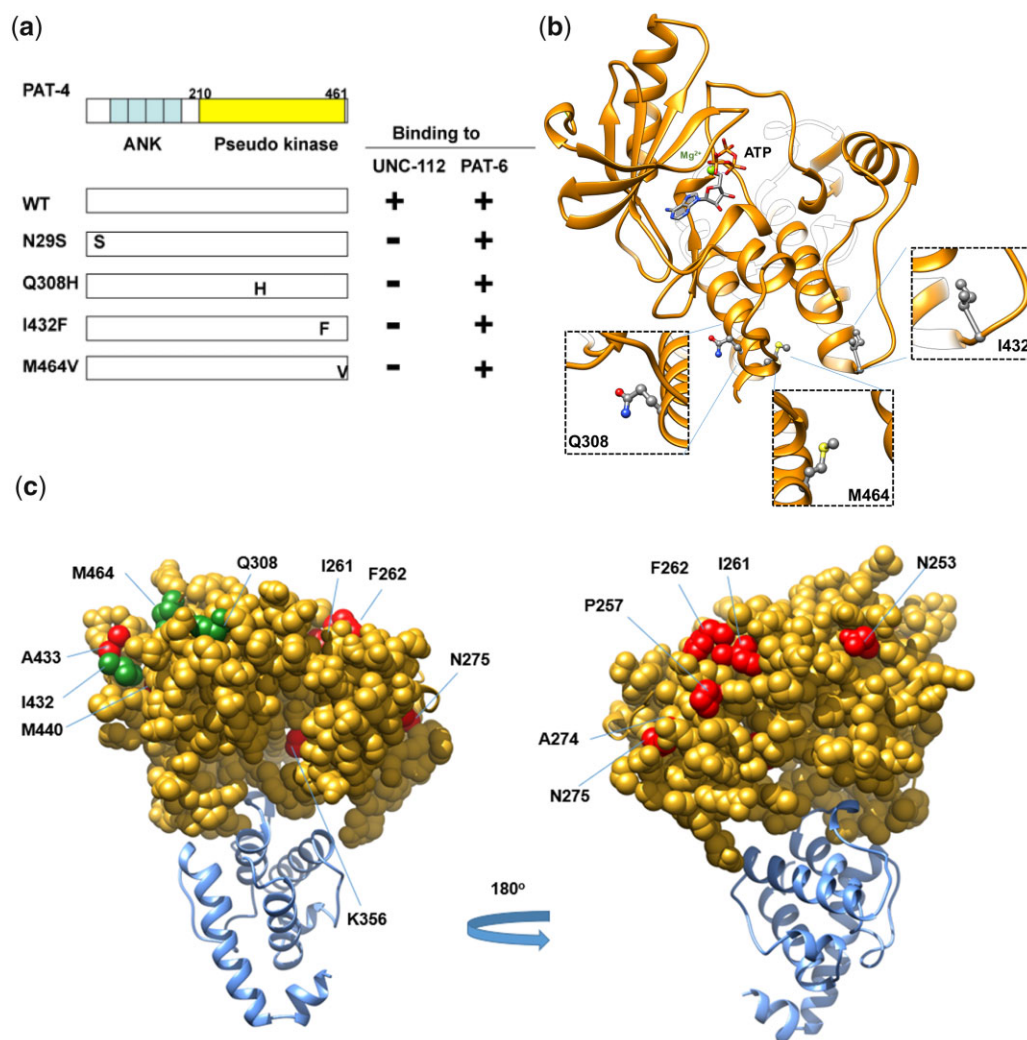
Fig. 1. Isolation of PAT-4 missense mutants that fail to interact with UNC-112. a) Schematic representation of domains in PAT-4 (ILK), location of mutations, and results of yeast 2-hybrid assays. "ANK" (ankyrin) and "Pseudo kinase" are domains predicted by PFAM. Numbers indicate amino acid residue numbers in PAT-4. + represents growth on His⁻ plate and Ade⁻ plate. – represents no growth on either His⁻ plate or Ade⁻ plate. Wild-type PAT-4 can bind to UNC-112 and PAT-6. PAT-4 with N29S, Q308H, I432F, or M464V cannot bind to UNC-112, but still can bind to PAT-6. WT denotes wild type. b) Homology model of PAT-4 structure based on the crystal structure of human ILK (PDB: 3KMW) (Fukuda *et al.* 2009) using Swiss-Model (Waterhouse *et al.* 2018), and showing the residues in the pseudo kinase domain that are mutated. The color scheme matches the colors of the domains in the schematic of part a. Three amino acid changes appearing in part a (Q308H, I432F, M464V) are shown in enlarged windows. c) Homology model of PAT-4 bound to the CH domain of PAT-6 based on the human ILK/α-parvin complex structure (3KMW.pdb; Fukuda *et al.* 2009) modelled with SWISS-MODEL (Waterhouse *et al.* 2018). PAT-4 kinase domain is shown in yellow in the space filling mode, the CH domain of PAT-6 is shown in dark cyan. The residues mutated in the 3 PAT-4 mutants identified here that fail to bind to UNC-112 (Q308H, I432F, M464V) are indicated in green. Residues that when mutated permit binding of PAT-4 to UNC-112 D382V (Qadota *et al.* 2014) are indicated in red. All of these residues mutated in PAT-4 are on a surface that is not covered by or does not overlap with the binding site for PAT-6 (α-parvin). This surface appears to have 2 clusters: 1 side with residues M440, I432, A433, M464, and Q308, and the other side with residues N275, A274, P257, F262, and I261.

suppressor mutant UNC-112 N-terminal clones. From suppressor screening of PAT-4 I432F, we isolated 14 suppressor mutant UNC-112 N-terminal clones (Table 2). Among the total of 20 suppressor mutant clones, there were 2 single amino acid changes, F301S and A96V (Table 2; Fig. 3a). Among remaining 18 mutant clones, there were 2 clones containing 2 mutations, m43-5-33 (N37S and S185T) and m22-4-9 (Q27R and F117S). To identify which single amino acid changes are critical for suppression, we created each single mutation by site-directed mutagenesis and then tested for PAT-4 Q308H or I432F binding using the yeast 2-hybrid assay. As a result, an UNC-112 N-terminal half with N37S showed binding to PAT-4 I432F, but UNC-112 N-terminal halves with the 3 other

single mutations did not show binding to PAT-4 Q308H or I432F. In the case of m43-5-33, since UNC-112N with N37S showed binding to PAT-4 I432F, S185T is not essential for suppression. In the case of m22-4-9, since UNC-112N with either Q27R or F117S alone did not show binding to PAT-4 Q308H, we concluded that 2 mutations (Q27R and F117S) are required together for binding to PAT-4 Q308H.

Taken together, we identified 4 sets of suppressor mutations; F301S, N37S, A96V, and Q27R plus F117S (Fig. 3a). Furthermore, all 4 mutation sets (F301S, N37S, A96V, and Q27R plus F117S) can bind to both PAT-4 Q308H and PAT-4 I432F. Previously (Qadota *et al.* 2020), we reported generating a homology model of UNC-112
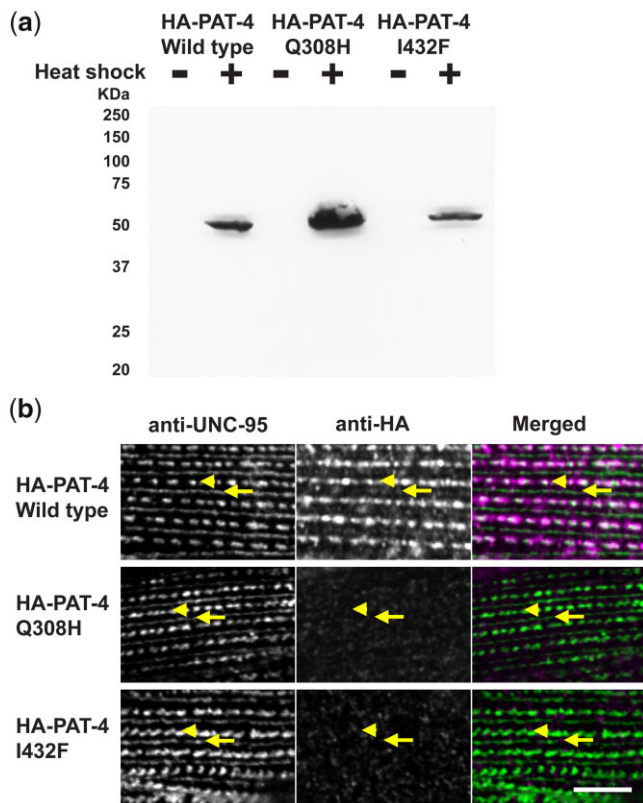
Fig. 2. PAT-4 Q308H and PAT-4 I432F mutant proteins that cannot bind to UNC-112 do not localize to integrin adhesion complexes. a) Western blot of lysates from transgenic nematodes carrying HA-tagged PAT-4 wild type, Q308H or I432F, expressed from a heat shock promoter, with heat shock (+) or without heat shock (−), reacted with anti-HA. Note that the apparently different level of expression of HA-PAT-4 is due to the variable rate of transmission of these extrachromosomal arrays in the different transgenic lines. b) Localization of heat shock-expressed HA-tagged PAT-4 wild type, Q308H, and I432F in transgenic animals. Worms were immunostained with anti-HA to detect the transgenic PAT-4 and with anti-UNC-95 to visualize the optical plane in body wall muscle cells that contain the integrin adhesion complexes (dense bodies and M-lines). Wild-type HA-PAT-4 localizes normally to dense bodies and M-lines. However, Q308H and I432F HA-PAT-4 fail to localize to these structures. Arrows indicate M-lines, and arrowheads indicate dense bodies. White bar, 10 μm.

based on the crystal structure of human kindlin-3 (Bu et al. 2020). We placed our single amino acid suppressor mutations on this model. In this model (Fig. 3b), N37, A96, and F301 are located along one side of UNC-112, fairly close together. N37 is located on a loop and the conservative substitution to serine, is predicted by Chimera to have minimal effect on local or global structure. Similarly, A96 is also located on a loop and the conservative substitution to valine is predicted to have minimal effect on the local or global structure of UNC-112. F301 is also located on a loop, and changing the large hydrophobic residue phenylalanine to the small polar residue serine is predicted to change the local but not global structure of UNC-112. Taken together, all 3 single amino acid changes seem to have no or minimal effect on the global structure of UNC-112, and are suggested to be involved in PAT-4 binding. Interestingly, the position of 1 suppressor mutation, F301, is next to the amino acid residue found in the PAT-4 nonbinding mutation, E302G [Qadota et al. 2021; Figs. 3c and 6 (with rectangle)], further highlighting the importance of the region F301-E302 in UNC-112 for PAT-4 binding. Finally, we note that
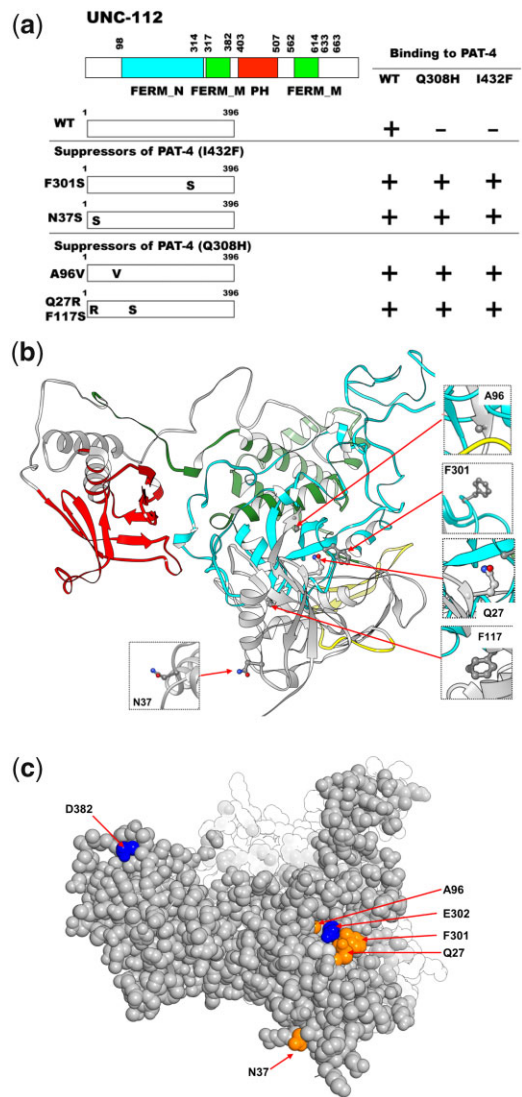

Fig. 3. Location of amino acid changes in UNC-112 suppressor mutant proteins that restore binding to PAT-4 (Q308H) and PAT-4 (I432F). a) Schematic representation of domains in UNC-112 (kindlin), location of mutations, and results of yeast 2-hybrid assays. FERM_N, FERM_M, and PH are domains predicted by PFAM. Numbers indicate amino acid residue numbers in UNC-112. + represents growth on His⁻ plate and Ade⁻ plate. − represents no growth on either His⁻ plate or Ade⁻ plate. Wild-type UNC-112 N-terminal half cannot bind to PAT-4 containing either Q308H or I432F mutations. UNC-112 N-terminal half with F301S, N37S, A96V, or Q27Q/F117S can bind to PAT-4 with Q308H and I432F. WT denotes wild type. b) Structure of UNC-112 (Qadota et al. 2020) based on the human kindlin-3 3D structure (PDB: 7C3M) (Bu et al. 2020) modelled with Swiss-Model (Waterhouse et al. 2018), and showing corresponding mutated residues. The color scheme matches the colors of the domains in the schematic of part a. Residues that were affected by amino acid changes appearing in part a (Q27, N37, A96, F117, and F301) are shown in enlarged windows. c) Space filling model of UNC-112 highlighting the location of the Q27, N37, A96, and F301 (in orange) identified in this study that when mutated restore the ability of PAT-4 Q308H and I432F mutants to bind to UNC-112, and D382 and E302 residues (in blue) that when mutated fail to bind to PAT-4 (Qadota et al. 2012, 2021).

although we could not find evidence that either Q27R or F117S alone can restore binding to PAT-4 mutants, Q27 lies in the same cluster of residues that contain A96, F301 and E302 (Fig. 3c). In contrast, F117 is located away from the surface and cluster of these UNC-112 suppressor and nonbinding mutants (Fig. 3b).
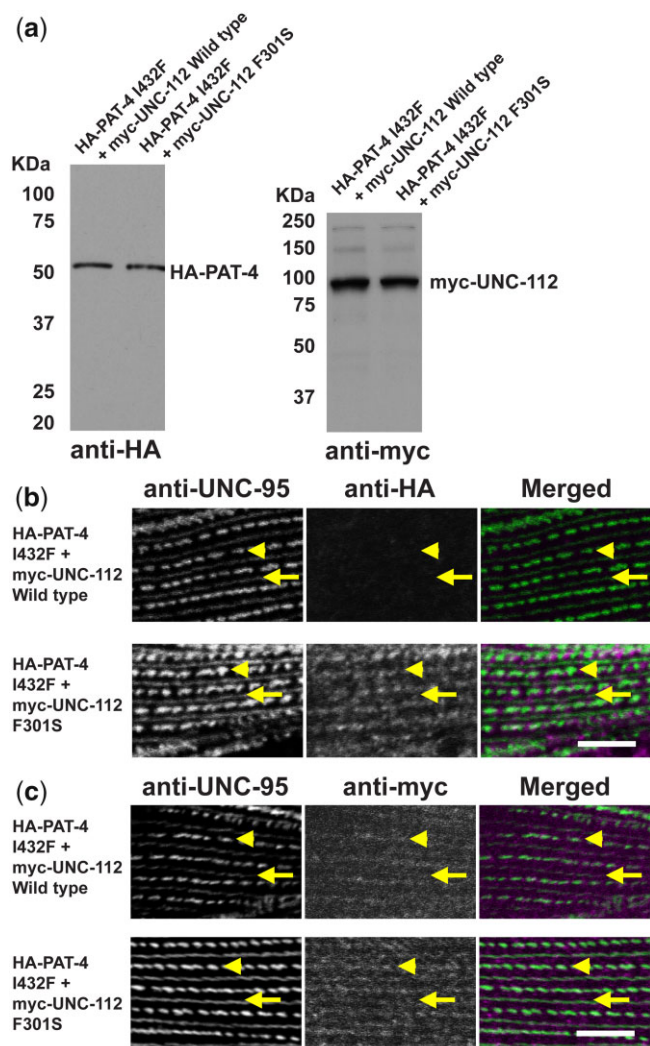
Fig. 4. Co-expression of HA-PAT-4 I432F and myc-UNC-112 F301S restores ability of PAT-4 I432F to localize to integrin adhesion sites. a) Western blot of lysates from transgenic worms expressing from a heat shock promoter HA-tagged PAT-4 I432F and either myc-tagged UNC-112 wild-type or UNC-112 F301S. Lysates were prepared after heat shock (+) and reacted with anti-HA or anti-myc antibodies. Expression of the HA- and myc-tagged proteins depended on heat shock. b) Localization of heat shock-expressed HA-tagged PAT-4 I432F in the presence of co-expressed myc-tagged UNC-112 wild type, or myc-tagged UNC-112 F301S. Adult worms were immunostained with anti-HA to detect transgenic PAT-4 and with anti-UNC-95 to visualize the optical plane of body wall muscle cells that contain dense bodies and M-lines (integrin adhesion sites). HA-PAT-4 I432F fails to localize to these structures in the presence of myc-UNC-112 wild type but does localize to these structures in the presence of myc-UNC-112 F301S. c) Localization of heat shock-expressed myc-tagged UNC-112 wild type or F301S in the presence of HA-tagged PAT-4 I432F. Adult worms were immunostained with anti-myc to detect transgenic UNC-112 and with anti-UNC-95 to visualize the optical plane of body wall muscle cells that contain dense bodies and M-lines (integrin adhesion sites). Both wild type and F301S UNC-112 localize to M-lines and dense bodies. For (b) and (c), yellow arrowheads mark dense bodies, whereas yellow arrows mark M-lines. White bar, 10 μm.

UNC-112 F301S can restore the ability of PAT-4 I432F to localize to M-lines and dense bodies in muscle

To examine whether UNC-112 F301S can restore the localization of PAT-4 I432F to muscle IACs, we created 2 transgenic lines: (i) co-expression in body wall muscle of HA-PAT-4 I432F and myc-

UNC-112 wild type and (ii) co-expression in body wall muscle of HA-PAT-4 I432F and myc-UNC-112 F301S. Heat shock induced expression of each protein in the 2 transgenic lines was demonstrated by western blot using antibodies to HA and myc (Fig. 4a). Myc-UNC-112 wild type and myc-UNC-112 F301S localize to dense bodies and M-lines similar to the localization of endogenous UNC-112 using anti-UNC-112 (Qadota *et al.* 2017) (Fig. 4c). We co-immunostained with anti-HA (to localize HA-PAT-4) and with anti-UNC-95 (to mark the IACs at M-lines and dense bodies). As indicated in Fig. 4b, it is clear that although myc-UNC-112 wild type fails to localize HA-PAT-4 I432F to IACs (similar to results in Fig. 2b), myc-UNC112 F301S can permit at least partial localization of HA-PAT-4 I432F to IACs in muscle.

Overexpression of PAT-4 I432F results in the disorganization of adhesion complexes at muscle cell boundaries and this disorganization is suppressed by co-expression of UNC-112 F301S

The PAT-4 I432F mutant protein cannot bind to UNC-112 but can bind to PAT-6 (Fig. 1). In addition, the PAT-4 I432F mutant protein cannot localize to any of the IACs in nematode muscle [M-lines and dense bodies (Fig. 2), or adhesion plaques at muscle cell boundaries (data not shown)], in the absence of the UNC-112 F301S suppressor mutant protein. We reasoned that if an excessive amount of PAT-4 I432F was expressed, PAT-4 I432F could bind to PAT-6, but because this PAT-4 I432F cannot bind to UNC-112, it would not localize to IACs, and thus, the amount of PAT-6 available to localize to IACs would be reduced. We tested this idea by heat shock (30°C for 24 h) induced overexpression of PAT-4 wild type, PAT-4 I432F and PAT-4 I432F/UNC-112 F301S, followed by immunostaining with anti-PAT-6 and imaging by both confocal and structured illumination microscopy (SIM). In wild-type worms, this heat shock treatment had no effect on the localization of PAT-6 to any of the IACs (M-lines, dense bodies or adhesion plaques at muscle cell boundaries; labeled wild type in Fig. 5) as imaged by confocal. At the higher resolution provided by SIM, the boundaries appear as a series of parallel diagonal lines. Overexpression of PAT-4 wild type also had no effect on muscle attachment structures (labeled OE: PAT-4 wild type in Fig. 5), as viewed by confocal and SIM. However, overexpression of PAT-4 I432F resulted in reduced accumulation of PAT-6 at the boundaries, and extra space between adjacent muscle cells as viewed by confocal (OE: PAT-4 I432F in Fig. 5). By SIM the boundaries appear more dot-like rather than parallel lines. Upon co-expression of UNC-112 F301S with PAT-4 I432F, the PAT-6 staining pattern was largely restored as seen by confocal, and by SIM the parallel lines at the boundary were mostly restored (OE: PAT-4 I432F + UNC-112 F301S in Fig. 5). In addition, we noticed a mild disruption of the organization of dense bodies by overexpression of PAT-4 I432F that was restored upon co-expression of UNC-112 F301S. In Fig. 5, for each strain, at the far right is a small box in which 2 adjacent dense bodies are seen by SIM. Note that all strains except for the 1 overexpressing PAT-4 I432F, show 2 distinct oval shapes.

Discussion
PAT-4 (ILK) protein surface that interacts with UNC-112 (kindlin)

The goal of this study was to obtain more information about an interacting surface between PAT-4 and UNC-112. Previously, we identified extragenic suppressor mutations in PAT-4 that restore binding to UNC-112 D382V [see Fig. 6 in which D382V (Qadota
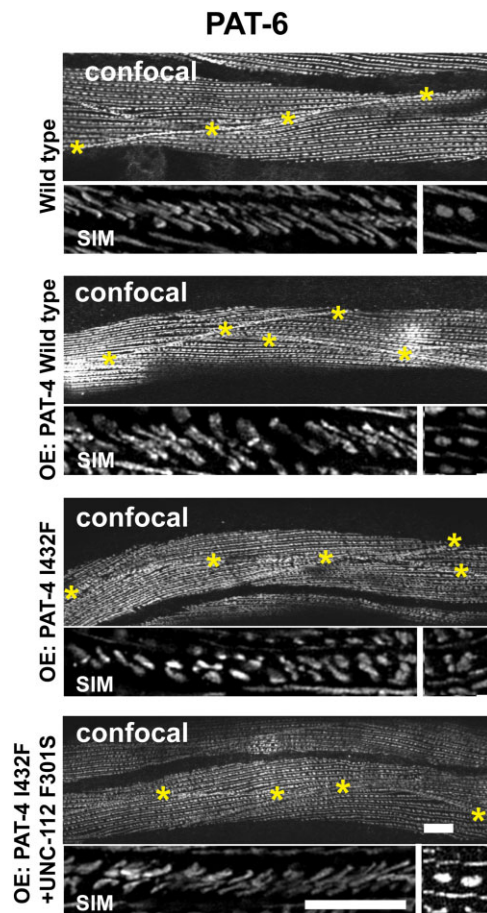
PAT-6

Fig. 5. Sustained overexpression of PAT-4 I432F results in disorganization of muscle cell boundary integrin adhesion complexes and this disorganization is suppressed by co-expression of UNC-112 F301S. Localization of PAT-6 (α-parvin) at M-lines, dense bodies, and muscle cell boundaries in wild-type worms, and worms carrying integrated arrays of PAT-4 wild type, PAT-4 I432F, and PAT-4 I432F + UNC-112 F301S. Young adult worms were exposed to 30°C 24 h, then fixed and immunostained with anti-PAT-6. For each strain, the top image was obtained using confocal microscopy (with yellow asterisks marking the muscle cell boundaries), and the lower 2 images were obtained using SIM. The major SIM image is a portion of a muscle cell boundary; the right-most box is a SIM image of a pair of dense bodies. By confocal imaging, overexpression of PAT-4 I432F results in reduced accumulation of PAT-6 at the boundaries, abnormal space between adjacent muscle cells, and a mild disruption of the structure of dense bodies. At the higher resolution and magnification provided by SIM, in wild type, the boundaries appear as a series of parallel diagonal lines. Upon overexpression of PAT-4 wild type, the boundaries appear like they do in wild type. However, overexpression of PAT-4 I432F results in more dot like structures. The parallel diagonal lines are restored upon co-expression of PAT-4 I432F and UNC-112 F301S. White bars 10 μm in confocal images and 5 μm in SIM images.

_et al._ 2012) is in blue font for UNC-112, and PAT-4 suppressors (Qadota _et al._ 2014) are in red font for PAT-4]. In a homology model of PAT-4, based on the ILK-parvin co-crystal structure (Fukuda _et al._ 2009), we had reported that residues mutated in the suppressors are located on 1 side of the PAT-4 protein, different from the surface of ILK (PAT-4) that binds to α-parvin (PAT-6) (Qadota _et al._ 2014). The 3 PAT-4 mutations that we have described here (see Fig. 6 in which Q308H, I432F, and M464V are in green font) that cannot bind to UNC-112, are also located on the same side of PAT-4 as are the 9 extragenic suppressor mutations (Fig. 1c). Thus, all of the residues mutated in PAT-4 that fail to

bind to UNC-112 or when mutated can restore binding to UNC-112 D382V are on a surface that is not covered by or does not overlap with the binding site for PAT-6 (α-parvin). Furthermore, this surface appears to have 2 clusters: 1 side with residues M440, I432, A433, M464, and Q308, and the other side with residues N275, A274, P257, F262, and I261. We hypothesize that these 2 clusters are crucial for interaction with UNC-112 (kindlin).

As we noted in Results, the I432F mutation results in nonbinding to UNC-112, whereas the next amino acid residue A433 when mutated to serine, restores binding to UNC-112 D382V (black rectangles for PAT-4 in Fig. 6), further suggesting that the surface of PAT-4 containing nonbinding and suppressor mutations is likely to be involved in binding to UNC-112. In the case of human ILK, since kindlin-2 L357 lies along the nonpolar face of an amphipathic helix important for ILK binding (Fukuda _et al._ 2014; Huet-Calderwood _et al._ 2014), it was hypothesized that a hydrophobic patch on ILK might be important for kindlin binding. Guided by this hypothesis, I427 of ILK was found to be essential for kindlin binding. Additional surface-exposed residues near I427 were tested for kindlin binding, and one of them, K423, was also found to be important for kindlin binding (Kadry _et al._ 2018). Corresponding to amino acid residues K423 and I427 in human ILK, are R438 and I442 in worm PAT-4. We should note that R438 and I442 are nearby one of the PAT-4 mutations described here that fail to bind to UNC-112, namely I432. For human ILK, the region corresponding to Q308 in PAT-4, has not yet been reported to be characterized.

UNC-112 (kindlin) protein surface that interacts with PAT-4 (ILK)

We have reported previously that the UNC-112 N-terminal half containing the FERM_N and part of the FERM_M domains binds to PAT-4 and that a missense mutation in the FERM_M domain (D382V) abolishes binding to PAT-4 (Qadota _et al._ 2012). For mammalian kindlin-2, it has been reported that the N-terminal half of FERM_M domain is responsible for binding to ILK, and that single amino acid changes in this region abolish binding to ILK (Fukuda _et al._ 2014). Recently, we reported that a missense mutation in the FERM_N domain of UNC-112, E302G, also results in diminished binding to PAT-4 (ILK) (Qadota _et al._ 2021), thus providing additional evidence that the FERM_N domain is critical for binding to PAT-4 (ILK). In the study reported here, we found that the mutations in UNC-112 that restore binding to PAT-4 Q308H or I432F, are also located in the FERM-N domain (F301), or N-terminal of the FERM-N domain (N37S and A96V)(in purple font for UNC-112 in Fig. 6). In fact, all 3 residues affected are located along the same side of UNC-112 in our homology model of UNC-112 (Fig. 3b). It is interesting to note that one of the suppressor mutations, F301S, resides in an amino acid next to E302, that when mutated to glycine cannot bind to PAT-4 (Qadota _et al._ 2021). As noted above, we obtained a similar result for PAT-4, _i.e._, PAT-4 I432F fails to bind to UNC-112 and yet PAT-4 A433S permits binding to UNC-112 D382V (which normally cannot bind to PAT-4 wild type). The previous data and data shown here expand the region and the residues of kindlin family proteins that are likely involved in the interaction with ILK.

PAT-4 binding to UNC-112 is required for the localization of PAT-4 to IACs

Loss of function mutations in _pat-4_ and _unc-112_ are Pat/embryonic lethal (Rogalski _et al._ 2000; Mackinnon _et al._ 2002), because a functioning myofilament lattice is not formed in embryonic muscle. Based on examining the localization of proteins in embryonic
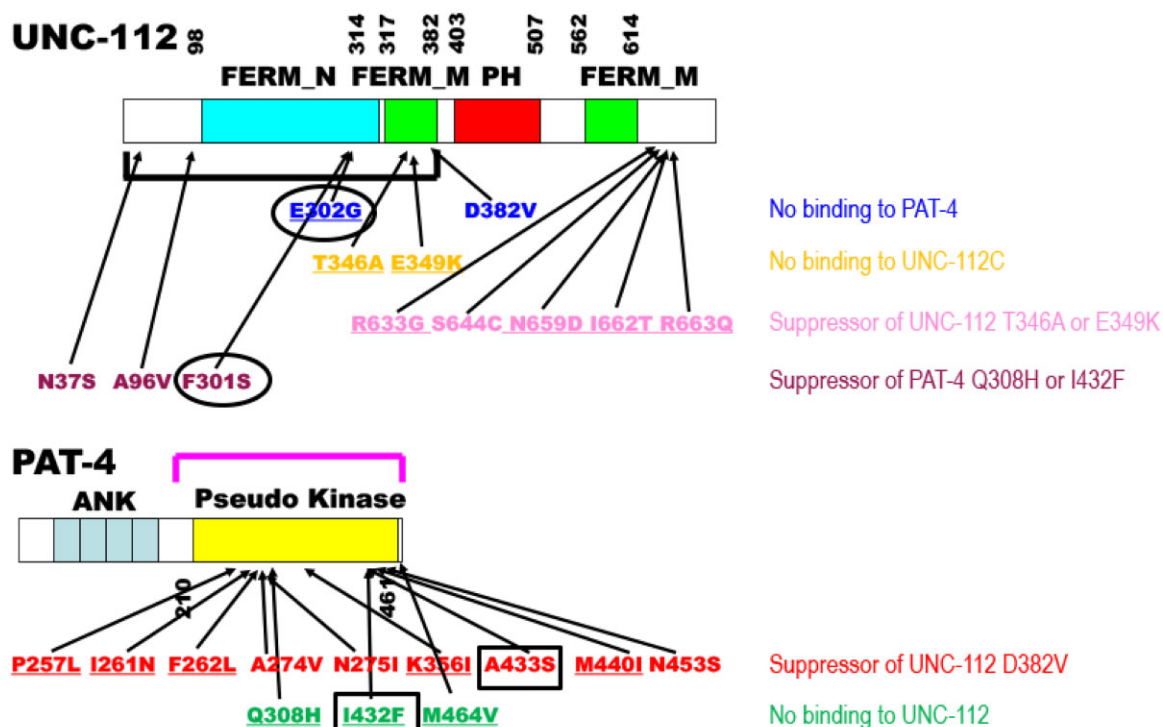
Fig. 6. Summary of single amino acid substitutions in UNC-112 and PAT-4 that affect intermolecular interaction between UNC-112 and PAT-4, and intramolecular interaction between the N- and C-terminal halves of UNC-112. Schematic representation of domains in UNC-112 (kindlin) and PAT-4 (ILK), location of mutations, and results of yeast 2 hybrid assays. "FERM_N," "FERM_M," "PH," "ANK," and "Pseudo kinase" are domains predicted by PFAM. Numbers indicate amino acid residue numbers in UNC-112 and PAT-4. The black bracket represents the region of UNC-112 that binds to PAT-4 (Mackinnon *et al.* 2002). The purple bracket represents the region of PAT-4 that binds to UNC-112 (Mackinnon *et al.* 2002). Blue amino acid changes in UNC-112 (D382V and E302G) are UNC-112 mutants that cannot bind to PAT-4 (Qadota *et al.* 2012, 2021). Orange amino acid changes are UNC-112 N-terminal mutants (T346A and E349K) that cannot bind to the UNC-112 C-terminal half (Qadota *et al.* 2012). Pink amino acid changes (R633G, S644C, N659D, I662T, and R663Q) restore the ability of UNC-112 N-terminal mutant proteins (T346A and E349K) to bind to the UNC-112 C-terminal half (Qadota *et al.* 2020). Purple amino acid changes in UNC-112 (N37S, A96V, and F301S) restore the ability of UNC-112 to bind to PAT-4 Q308H or I432F (this study). Red amino acid changes in PAT-4 (P257L, I261N, F262L, A274V, N275I, K366I, A433S, M440I, N453S) restore the ability of PAT-4 to bind to UNC-112 D382V (Qadota *et al.* 2014). Green amino acid changes in PAT-4 (Q308H, I432F, and M464V) result in PAT-4 that cannot bind to UNC-112 (this study). Underlining represents conserved amino acid residues (UNC-112 for kindlin and PAT-4 for ILK). Black circles in UNC-112 (around E302G and F301S) and black rectangles in PAT-4 (around A433S and I432F) indicate that a nonbinding mutation and a suppressor mutation are located in consecutive amino acid residues.

muscle of dying *pat-4* and *unc-112* embryos, it has been demonstrated that PAT-4 is required for proper localization of UNC-112, and that UNC-112 is required for proper localization of PAT-4 (Mackinnon *et al.* 2002). In adult *C. elegans* muscle cells, by expressing an HA-tagged UNC-112 mutant (D382V) protein that cannot bind to PAT-4, it was shown that PAT-4 binding to UNC-112 is required for UNC-112 to localize to IACs (M-lines and dense bodies) (Qadota *et al.* 2012). In this study, we isolated PAT-4 mutants that cannot bind to UNC-112, and expressed those 2 mutant PAT-4 proteins in adult *C. elegans* muscles and found that UNC-112 binding is required for PAT-4 localization to IACs (Fig. 2). Furthermore, we found that co-expression of a mutant (F301S) UNC-112 protein that restores binding to mutant PAT-4 (I432F), also restores the localization of the mutant PAT-4 to IACs (Fig. 4). Similar results have been reported for human ILK. Human ILK with either K423D or I427E in the pseudo kinase domain (Supplementary Fig. 1) could not localize to focal adhesions of CHO cells (Kadry *et al.* 2018). Neither the PAT-4 mutants nor the ILK mutants showed an obvious defect in protein stability (Fig. 2; Kadry *et al.* 2018). Our PAT-4 mutant proteins cannot bind to UNC-112 but still can bind to PAT-6 (α-parvin) (Fig. 1), indicating that the overall structure and stability of the PAT-4 mutant proteins are intact. Moreover, since our 4 PAT-4 mutant proteins have amino acid changes in the pseudo kinase domain (Q308H,

I432F, M464V), or in the N-terminus (N29S), and not in the ankyrin repeat region which is known to bind to UNC-97 (PINCH) (Mackinnon *et al.* 2002; Norman *et al.* 2007), suggesting that these PAT-4 mutant proteins, when co-expressed with suppressor mutant UNC-112 (F301S) protein can still form a complete 4 protein complex (UNC-112/PAT-4/PAT-6/UNC-97) in vivo. Since we previously demonstrated by co-pelleting from worm extracts that UNC-112 (kindlin), PAT-4 (ILK), PAT-6 (α-parvin) and UNC-97 (PINCH) form a tight complex (Qadota *et al.* 2014), we propose the name, "KIPP complex," for this 4-protein complex.

IACs at muscle cell boundaries are more dynamic than M-lines and dense bodies

C. elegans muscle cells attach to extracellular matrix through 3 structures: M-lines, dense bodies, and adhesion plaques at muscle cell boundaries (Qadota *et al.* 2017). These 3 attachment structures contain different sets of proteins, but a number of proteins are in common, including PAT-3 (β-integrin), UNC-112 (kindlin), PAT-4 (ILK), PAT-6 (α-parvin), UNC-97 (PINCH), and UNC-95, that are located near the muscle cell membrane. In this study, we reported that overexpression of PAT-4 I432F, that cannot bind to UNC-112, results in disorganization of muscle cell boundaries and mild disorganization of dense bodies (Fig. 5). Note that over-expression of PAT-4 I432F was conducted in a wild type

background in which endogenous PAT-4 is also expressed, and therefore the observed phenotype is gain of function or neomorphic. Nevertheless, the structures affected from this experiment overlap the known localization of PAT-4 in wild-type muscle (M-lines, dense bodies and muscle cell boundaries). We interpret these results in the following way: PAT-4 I432F binds to PAT-6, but this PAT-4/PAT-6 complex cannot localize to attachment structures due to PAT-4 I432F's inability to bind to UNC-112, and as a result, the amount of PAT-6 available to localize to adhesion complexes is reduced. The reduced level of PAT-6 results in less downstream proteins at these structures. In fact, although the null state for *pat-6* is Pat (paralyzed and arrested at 2-fold) embryonic lethal (Lin *et al.* 2003), *pat-6* RNAi beginning from the L1 larval stage results in disorganization of adult myofibrils (unpublished data). In addition, the effect of PAT-4 I432F overexpression was limited to muscle cell boundaries and dense bodies (somewhat), but not to M-lines. Our previous study suggests that the adhesion plaques at muscle cell boundaries are more dynamic than dense bodies or M-lines (Moody *et al.* 2020): PIX-1 is a Rac GEF that is localized to all 3 integrin adhesion structures (M-lines, dense bodies and boundaries), but is only required at muscle cell boundaries. Either loss of function or overexpression of PIX-1 results in the same cell boundary defect (Moody *et al.* 2020), suggesting that cell boundary structures require rapid turnover of component proteins, and is more dynamic than M-lines and dense bodies. In the future, we might be able to test this hypothesis by measuring and comparing protein exchange rates at the cell boundary, dense bodies and M-lines by, for example, FRAP analysis.

Genetic analysis of the UNC-112 to PAT-4 interaction

Figure 6 summarizes our results to date using a random mutagenesis approach (Qadota and Benian 2014) to isolate nonbinding mutants and their intragenic and extragenic suppressor mutants (Qadota *et al.* 2012, 2014, 2020, 2021; this study). Other than deletion and nonsense mutations, there are reports about 2 *unc-112* alleles (no reports for *pat-4*): first, the Unc allele, *unc-112(r367)*, is a missense mutation, T85I (Rogalski *et al.* 2000). The molecular nature of UNC-112 T85I has not been examined, and thus, we do not know if the phenotype is due to modified binding to PAT-4 or PAT-3, or whether it results in a unstable protein. Second, there is 1 unusual allele created by CRISPR/Cas9, *unc-112(kq715)*, L715E, near the end of protein, which shows a defect in the migration of the distal tip cell (Park *et al.* 2020), but whether there was an effect on the attachment structures of body wall muscle, was not reported. Using this accumulated set of mutations that affect interaction between UNC-112 and PAT-4, we can roughly estimate the binding surface between these 2 proteins, and key residues of each protein responsible for this interaction. However, to clarify the binding surface definitively, analysis of a co-crystal structure of UNC-112 (kindlin) and PAT-4 (ILK) will be required, and so far, no such co-crystal structure for any kindlin/ILK pair has been reported. Hopefully, our mutational analysis will be of some use to validate co-crystal structures. Moreover, we have not yet explored the in vivo phenotype of the mutations in *unc-112* and *pat-4* shown in Fig. 6, but we showed reduced localization of PAT-4 and UNC-112 proteins and the deleterious effects of mutant PAT-4 and UNC-112 proteins in adult muscle (this study; Qadota *et al.* 2012). Since both UNC-112 and PAT-4 require each other (Mackinnon *et al.* 2002), individual homozygous mutations might result in Pat/embryonic lethality, but in the presence of a suppressor mutation, the worms might bypass the embryonic

lethality and either display an adult Unc phenotype or appear like wild type. In the future, using CRISPR/Cas9 technology, we hope to create homozygous nonbinding mutants with or without homozygous suppressor mutations and then examine for embryonic and adult stage muscle defects. Through this type of in vivo genetic analysis, we would be able to reveal the in vivo meaning of the interaction of UNC-112 and PAT-4 in the excellent genetic model, *C. elegans*.

Data availability

Worm and yeast strains, and plasmids are available upon request. The authors affirm that all data necessary for confirming the conclusions of the article are present within the article, figures, and tables.

Supplemental material is available at *G3* online.

Conflicts of interest

None declared.

Literature cited

Bu W, Levitskaya Z, Loh ZY, Jin S, Basu S, Ero R, Yan X, Wang M, Ngan SFC, Sze SK, *et al.* Structural basis of human full-length kindlin-3 homotrimer in an auto-inhibited state. PLoS Biol. 2020; 18(7):e3000755.

Fukuda K, Bledzka K, Yang J, Perera HD, Plow EF, Qin J. Molecular basis of kindlin-2 binding to integrin-linked kinase pseudokinase for regulating cell adhesion. J Biol Chem. 2014;289(41): 28363–28375.

Fukuda K, Gupta S, Chen K, Wu C, Qin J. The pseudoactive site of ILK is essential for its binding to alpha-Parvin and localization to focal adhesions. Mol. Cell. 2009;36(5):819–830.

Gieseler K, Qadota H, Benian GM. Development, structure and maintenance of C. elegans body wall muscle. In: The C. elegans Research Community, editor. WormBook; 2017. doi/10.1895/-wormbook.1.81.2.

Hannak E, Oegema K, Kirkham M, Gönczy P, Habermann B, Hyman AA. The kinetically dominant assembly pathway for centrosomal asters in Caenorhabditis elegans is gamma-tubulin dependent. J Cell Biol. 2002;157(4):591–602.

Hobert O, Moerman DG, Clark KA, Beckerle MC, Ruvkun G. A conserved LIM protein that affects muscular adherens junction

integrity and mechanosensory function in Caenorhabditis elegans. J Cell Biol. 1999;144(1):45–57.

Huet-Calderwood C, Brahme NN, Kumar N, Stiegler AL, Raghavan S, Boggon TJ, Calderwood DA. Differences in binding to the ILK complex determines kindlin isoform adhesion localization and integrin activation. J. Cell Sci. 2014;127:4308–4321.

Kadry YA, Huet-Calderwood C, Simon B, Calderwood DA. Kindlin-2 interacts with a highly conserved surface of ILK to regulate focal adhesion localization and cell spreading. J. Cell Sci. 2018;131: jcs221184.

Kelley LA, Mezulis S, Yates CM, Wass MN, Sternberg MJ. The Phyre2 web portal for protein modeling, prediction and analysis. Nat Protoc. 2015;10(6):845–858.

Lin X, Qadota H, Moerman DG, Williams BD. C. elegans PAT-6/actopaxin plays a critical role in the assembly of integrin adhesion complexes in vivo. Curr. Biol. 2003;13(11):922–932.

Mackinnon AC, Qadota H, Norman KR, Moerman DG, Williams BD. C. elegans PAT-4/ILK functions as an adaptor protein within integrin adhesion complexes. Curr Biol. 2002;12(10):787–797.

Mitani S. Genetic regulation of mec-3 gene expression implicated in the specification of the mechanosensory neuron cell types in Caenorhabditis elegans. Dev Growth Differ. 1995;37(5):551–557.

Moerman DG, Fire A. In: DL Riddle, T Blumenthal, BJ Meyer, JR Priess, editors. Muscle structure, function and development. C. elegans II. Cold Spring Harbor (NY): Cold Spring Harbor Laboratory Press; 1997. p. 417–470.

Moerman DG, Williams BD; The C. elegans Research Community. Sarcomere assembly in C. elegans muscle. In: The C. elegans Research Community, editor. WormBook; 2006. p. 1–16. doi: 10.1895/wormbook.1.81.1.

Moody JC, Qadota H, Reedy AR, Okafor CD, Shanmugan N, Matsunaga Y, Christian CJ, Ortlund EA, Benian GM. The Rho-GEF PIX-1 directs assembly or stability of lateral attachment structures between muscle cells. Nat Commun. 2020;11(1):5010. doi: 10.1038/s41467-020–18852-4.

Nonet ML, Grundahl K, Meyer BJ, Rand JB. Synaptic function is impaired but not eliminated in C. elegans mutants lacking synaptotagmin. Cell. 1993;73(7):1291–1305.

Norman KR, Cordes S, Qadota H, Rahmani P, Moerman DG. UNC-97/PINCH is involved in the assembly of integrin cell adhesion complexes in Caenorhabditis elegans body wall muscle. Dev Biol. 2007;309(1):45–55.

Park A, Qiu Z, Bumm J, Lee M. A novel mutation in unc-112/kindlin locus causes distal tip cell migration defects. microPubl Biol. 2020. doi:10.17912/micropub.biology.000265.

Pettersen EF, Goddard TD, Huang CC, Couch GS, Greenblatt DM, Meng EC, Ferrin TE. UCSF Chimera–a visualization system for exploratory research and analysis. J Comput Chem. 2004;25(13):1605–1612.

Qadota H, Mercer KB, Miller RK, Kaibuchi K, Benian GM. Two LIM domain proteins and UNC-96 link UNC-97/pinch to myosin thick filaments in Caenorhabditis elegans muscle. Mol Biol Cell. 2007;18(11):4317–4326.

Qadota H, Moerman DG, Benian GM. A molecular mechanism for the requirement of PAT-4 (integrin-linked kinase (ILK)) for the localization of UNC-112 (Kindlin) to integrin adhesion sites. J Biol Chem. 2012;287(34):28537–28551.

Qadota H, Benian GM. An approach for exploring interaction between two proteins in vivo. Front Physiol. 2014;5:162.

Qadota H, Luo Y, Matsunaga Y, Park AS, Gernert KM, Benian GM. Suppressor mutations suggest a surface on PAT-4 (Integrin-linked Kinase) that interacts with UNC-112 (Kindlin). J Biol Chem. 2014;289(20):14252–14262.

Qadota H, Matsunaga Y, Nguyen KCQ, Mattheyses A, Hall DH, Benian GM. High-resolution imaging of muscle attachment structures in Caenorhabditis elegans. Cytoskeleton. 2017;74(11):426–442.

Qadota H, Luo Y, Oberhauser AF, Benian GM. Genetic analysis of the interaction between the N- and C-terminal halves of UNC-112 (kindlin). microPubl Biol. 2020. doi:10.17912/micropub.biology.000342.

Qadota H, Oberhauser AF, Benian GM. Missense mutation of a conserved residue in UNC-112 (kindlin) eliminates binding to PAT-4 (ILK). microPubl Biol. 2021. doi:10.17912/micropub.biology.000454.

Rogalski TM, Mullen GP, Gilbert MM, Williams BD, Moerman DG. The UNC-112 gene in Caenorhabditis elegans encodes a novel component of cell-matrix adhesion structures required for integrin localization in the muscle cell membrane. J Cell Biol. 2000;150(1):253–264.

Takita Y, Takahara M, Nogami S, Anraku Y, Ohya Y. Applications of the long and accurate polymerase chain reaction method in yeast molecular biology: direct sequencing of the amplified DNA and its introduction into yeast. Yeast. 1997;13(8):763–768.

Warner A, Xiong G, Qadota H, Rogalski T, Vogl AW, Moerman DG, Benian GM. CPNA-1, a copine domain protein, is located at integrin adhesion sites, and is required for myofilament stability in C. elegans. Mol Biol Cell. 2013;24(5):601–616.

Waterhouse A, Bertoni M, Bienert S, Studer G, Tauriello G, Gumienny R, Heer FT, de Beer TAP, Rempfer C, Bordoli L, *et al.* SWISS-MODEL: homology modelling of protein structures and complexes. Nucleic Acids Res. 2018;46(W1):W296–W303.

Waterston RH. Muscle. In: WB Wood, editor. The Nematode Caenorhabditis elegans. Cold Spring Harbor (NY): Cold Spring Harbor Laboratory Press; 1988. p. 281–335.

Williams BD, Waterston RH. Genes critical for muscle development and function in Caenorhabditis elegans identified through lethal mutations. J Cell Biol. 1994;124(4):475–490.

Wilson KJ, Qadota H, Benian GM. Immunofluorescent localization of proteins in Caenorhabditis elegans muscle. Methods Mol Biol. 2012;798:171–181.

Yochem J, Gu T, Han M. A new marker for mosaic analysis in Caenorhabditis elegans indicates a fusion between hyp6 and hyp7, two major components of the hypodermis. Genetics. 1998;149(3):1323–1334.